ELSEVIER

Journal of Materials Processing Technology 117 (2001) 226–237

Journal of Materials Processing Technology

www.elsevier.com/locate/jmatprotec

A novel approach to operating force evaluation in high strain rate metal-deforming technological processes

V.P. Astakhov*, S.V. Shvets

Hyper Tool Engr Co, 3319 Fulham Dr., Rochester Hills, MI 48309, USA

Accepted 5 September 2001

Abstract

One of the major problems that exist in verifying metal-forming force models is a significant scatter in the measurements of the actual process force(s). This is essentially true for any high-energy rate forming process, which involves high strain, high strain rate and high process temperature. Owing to the fact that any energy propagates in waves, this paper suggests that the interaction of the energy waves might affect the actual process force(s). A novel concept of interaction between the deformation and heat waves has been studied. The metal-cutting process was selected as a test process because it involves a combination of extremely high strain rates, large strains and high temperatures. The experimental results obtained from bar turning tests prove the proposed concept by revealing the existence of reinforcements and interferences as the result of interactions of the heat and deformation waves. The influence of the process parameters on this interaction is also studied.

Keywords: High strain rate deformation processes; Coherent energy waves; Reinforcements and interferences of energy waves; Metal cutting; Cutting force

1. Introduction

The importance of metals in modern technology is due to the ease with which they may be formed into useful shapes such as tubes, rods and sheets [1]. Useful shapes may be generated in two basic ways:

1. By plastic deformation processes in which the volume and mass of metal are conserved and the metal is displaced from one location to another.
2. By metal removal or machining processes in which material is removed in order to give it the required shape.

Hundreds of processes have been developed for specific metalworking applications. These processes may be broadly classified into two categories on the basis of the strain rate involved as follows:

1. Processes utilizing high plastic strain rates ($\dot{\varepsilon} \leq 1\,\mathrm{s}^{-1}$).
2. Processes utilizing moderated plastic strain rates ($\dot{\varepsilon} < 1\,\mathrm{s}^{-1}$).

As known [1], many of the modern metalworking operations utilize high plastic strain rates. As a result, the mechanical properties of the work material obtained in the standard mechanical tests should be modified for the analysis of such operations [2]. The treatment of this subject matter has appeared in a number of recent studies and the current literature bears witness to the fact that the body of knowledge in this field has grown enormously. Solutions by costly trial-and-error methods of yesterday can be obtained today by making use of the scientific approach. Thus, empirical prediction of the forming variables, such as power and forces, is replaced by the results from studies of the mechanics of the process and application of sound theories of plasticity [2].

The application of sound theories of plasticity requires, however, a satisfactory test method for the so-called ''high-energy rate forming'' where high rates of deformation and high temperatures combined with large strains may occur. One of these processes is metal cutting where reportedly high strain rates (of the order 10^3–$10^6\,\mathrm{s}^{-1}$ [3–6]) and high temperatures (600–800°C [3–6]) are the case. Therefore, if the strain rate encountered in metal-cutting process is high and can be adequately determined, then metal cutting may become a very important testing method for the determination of the dynamic physical properties of work materials. Such a possibility was suggested by Lira and Thomsen [6] and Shaw [4].

One of the major outputs of any metal-deforming process and thus of metal cutting is the force required to deform or

* Corresponding author. Tel.: +1-810-226-5155; fax: +1-810-263-4571.
E-mail addresses: astvik@mailcity.com, astakhov@nachimtc.com (V.P. Astakhov).

0924-0136/01/$ – see front matter
PII: S0924-0136(01)01103-7

cut the workpiece. Knowing such a force, one can determine the power needed to accomplish the process. This paper concerns with the problem of determining the cutting forces.

Three major traditional approaches to the determination of the thermomechanical behavior of work materials (and thus to the determination of the cutting force) in cutting may be distinguished as follows [7]:

1. The high strain, strain rate and temperature occurring in metal cutting do not affect the mechanical properties of workpiece materials so that the stress–strain curves obtained in the standard mechanical tests can be used in the determination of the work material resistance to cutting, and thus the calculation of the cutting force. Multiple experimental results to prove such a point have been reported [3–5,8,9–11].
2. High strain, strain rate and/or their linear/non-linear combination affect the resistance of the work material to cutting (the shear flow stress, as believed), and thus to calculate the cutting force, the thermomechanical properties of workpiece materials obtained in the standard tensile test should be correspondingly modified [2,12–14]. According to this approach, the stress–strain relationships obtained in the standard tensile test cannot be used in metal cutting. Instead, a number of new stress–strain relationships mostly obtained from the work on material properties under high strain rate conditions have been proposed [12–14].
3. The essence of the third approach is the belief that the shear flow stress of the work material (always considered as the major mechanical characteristic of the work material in the cutting process) is affected by the combined influence of strain hardening (a function of the strain and strain rate) and thermal-softening (a function of the process temperature). As before, a number of new stress–strain relations have been proposed to calculate the cutting force [15–19], and numerous theoretical and experimental proofs have been provided to support this approach.

The most amazing fact is that these three approaches somehow coexist. Moreover, the authors supporting the first approach (for example [5]) tried to find experimentally the influence of strain, strain rate and process temperature on the work material resistance to cutting but did not succeed. The need is felt to explain what causes the scatters in the experimental results that support these three approaches.

The traditional way to conduct experimental studies is to measure the cutting force experimentally. The problem in such measurements is chatter, which may be thought of as quite violent cutting fluctuations [4,5]. Different averaging techniques are used to process cutting force signals in practice [20]. Because the dynamic system properties, system respond of the measuring rig and the averaging technique (including cut-off frequencies of transducers, band filters, etc.) are normally not reported; one can find sufficient proofs for any theory or approach. As an extreme, a special

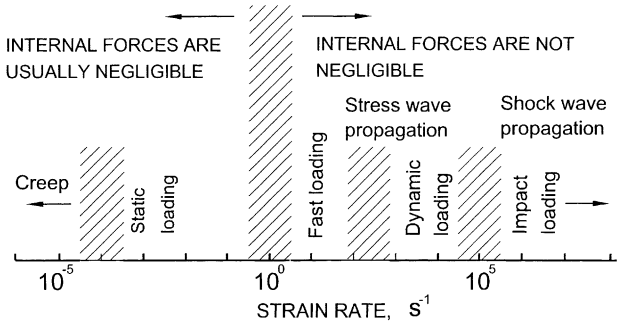

Fig. 1. Classification of various types of loading in terms of strain rate.

group of experimental studies conducted over the last 20 years claims that the cutting force has stochastic nature (well discussed in [20]). As a result, the cutting process is classified as a stochastically stationary process so that its prediction cannot be made on the basis of its theoretical analysis.

In the authors' opinion, the scatter in the reported experimental results on cutting force measurements is caused by ignoring wave effects in the deforming of metals at high strain rates. To be specific, consider classification of various types of loading in terms of the strain rate as shown in Fig. 1 [20]. Upon examining the present state of research within the individual areas indicated in this figure, it can be found that for strain rates of less that $10\ s^{-1}$, reliable, commercially available experimental apparatus and standard methods for the evaluation of results already exist. A rather different situation appears at higher strain rates (greater than about $10^4\ s^{-1}$). As can be seen from Fig. 1, the role of material internal forces cannot be neglected in this region. Nevertheless, Oxley [2] and many other researchers just neglected these forces in their analyses reporting, simultaneously, extremely high strain rates in metal cutting. Moreover, when the rate of strain falls in this region, a description of the corresponding force effects must unavoidably include the propagation of the stress waves and/or stress pulse [21]. Unfortunately, this fact has never been considered in metal cutting or in any high-energy rate forming process.

The purpose of this paper is to introduce interaction between the deformation and heat waves in deformation of metals at high strain rates as a phenomenon, which occurs in high-energy rate metal forming and affects the process parameters.

2. The basic concept

The basic concept of the proposed approach is based on the system concept in metal cutting [22] and stems from the definition of Truesdell and Noll [23] according to which a wave is considered as the means by which a given system state moves to another with finite velocity. Bearing in mind this definition, the basic concept may be described as follows. Machining results in the generation of deformation waves in the workpiece. This process also involves high

strains and, as a result, high rates of heat generation. Since the generated heat is transferred from one point to another in waves, it is logical to assume that the deformation and the heat waves may interact so that the process parameters might be affected. The main process parameter is the force involved. Therefore, the force should vary with the phase difference between the above-mentioned waves since they are coherent as formed in the workpiece by the same source, namely by the cutting tool.

Since, it is next to impossible to propose a suitable theory for a complex deformation process that is valid for both arbitrary time and arbitrary space parameters [24], the basic concept has been verified experimentally.

3. Experimental verification

3.1. Why metal cutting as a test?

The metal-cutting process was selected as a test method for the reasons well discussed in [4,6,20]. The attraction of metal cutting lies in the fact that the process involves a combination of high strain rates, $\dot{\varepsilon} = 10^2 - 10^4\ s^{-1}$ (although significant higher strain rates are commonly reported [2,3], strain rates beyond the indicated range is just a matter of imagination as well discussed in [20]), large strains, $\varepsilon \geq 2$, and most of the energy input during the metal-cutting process converts into heat which is then transferred into the chip, the workpiece and the cutting tool.

These extreme conditions of deformation of the work material in an ordinary cutting operation are immediately apparent if one compares them with other known methods. Thus, for instance, in the standard tensile test, where $\dot{\varepsilon} = 10^{-3}\ s^{-1}$ or even in a rapid impact type tensile test, where $\dot{\varepsilon} = 10^3\ s^{-1}$, the strain rates are considerably below those of conventional metal cutting. Moreover, in a tension test, the specimen displays the undesirable behavior of necking so that the test results are subjected to complicated corrections [25]. Finally, fracture will limit the extent of the deformation available, which ordinarily is of the order of 50% reduction of the specimen's cross-sectional area.

There are a number of known rapid tests where necking does not occur or where it may be avoided [26]. Among them are the rapid torsion test, the uniaxial rapid impact test, the upsetting test. However, the strain rates, strains and temperature ranges in these tests are much below those commonly found in metal cutting. Moreover, a metal-cutting test can be carried out in such a manner that the forces and other variables can be measured with relatively high accuracy [20]. Therefore, a metal-cutting test was selected to verify the adopted assumptions.

3.2. Test conditions

Since the dynamic parameters of metal cutting are known to be very sensitive to relatively small changes in the cutting process [20], a special attention was paid to the selection of the conditions of the tests and to the experimental methodology. The test conditions were selected as follows:

1. *Workpiece material*. Hot finished "triple alloy" steel AISI 4140 was used. The composition, the element limits and the deoxidation practice were selected according to the requirements of standard ANSI/ASME B94.55M-1985 and were requested from the steel dealer. The actual chemical composition has been analyzed using LECO® SA-2000 discharge-optical emission spectrometer. The results were compared with those obtained from the dealer. The actual chemical composition was 0.39% C, 0.72% Mn, 0.012% P, 0.001% S, 0.31% Si, 1.03% Cr, 0.16% Mo. The hardness of the work material was 221 HB and it has been determined over the complete cross-section of the terminal end and working length of each bar workpiece used in the tests. Cutting tests were conducted only on the bars where the hardness was within the limits ±10%. Special metallurgical parameters such as the element counts, microstructure, grain size, inclusions count, etc. were inspected using quantitative metallography [20].
2. *Machine*. A retrofitted Schaerer HPD 631 lathe was used. The drive unit motor was replaced with a 15 kW variable speed AC motor and the feed motor was replaced with a 5 kW variable speed AC motor. The motors were individually controlled by AC inverters. The AC inverters are designed to provide required volts/hertz ratio allowing the AC motors to run at their optimum efficiency and provide rated torque capability through the motor's rated base speed. The control section of the AC inverters consists of a control board with a 16-bit microprocessor and keypad interface with an 8-bit microprocessor.
3. *Cutting tool*. A general purpose tool holder CTJNR2520L16 and cutting inserts made of P20 (8% Co, 15% TiC, 77% WC) general purpose carbide were used. The geometry parameters of the tool were controlled according to American National Standard B94.50-1975. Tolerances for all angles were ±0.5°. The roughness R_a of the tool face and flank did not exceed 0.25 μm and was measured according to American National Standard ANSI B46.1-1978. Each cutting edge was examined at magnification of 15× for visual defects as chip or cracks.
4. *Dynamometer*. A two-component Kistler Type 9271A dynamometer was used. Based on the standard mounting as specified by the supplier (Kistler), the load washer (Kistler Type 9065) was installed in the dynamometer and pre-loaded to 120 kN. At this pre-load, the range for force measurements is from −20 to +20 kN, threshold is 0.02 N, sensitivity is −1.8 pC/N, linearity does not exceed a range of ±1.0% FSO, overload is 144 kN, cross-talk does not exceed 0.02 N/N, resonant frequency is 40 kHz, temperature error does not exceed +30 N/°C.

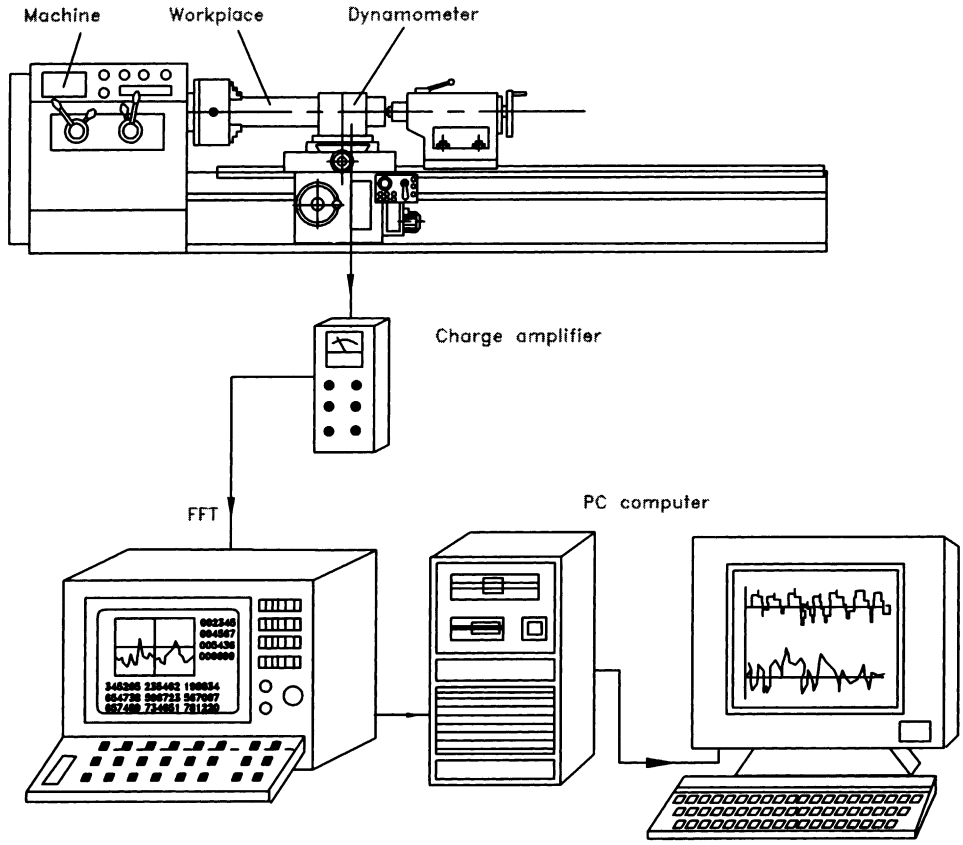

Fig. 2. Schematic diagram for measuring setup.

5. *Measuring setup*. A schematic diagram of the setup used in the experiments is shown in Fig. 2. The load washer was connected to the charge amplifiers (Kistler, Mod. 5004). The charge amplifier (Type 5004) is a mains-operated DC amplifier of very high input impedance with capacitive negative feedback, intended to convert the electric charge from a piezoelectric transducer into a proportional voltage on the low impedance amplifier output. The calibration factor setting (adjustment of transducer sensitivity at the amplifier) makes standardized amplifier sensitivities of, for example, 1, 2, 5 mV, etc. per mechanical unit (N) possible. The carefully designed calculating disc enables the reciprocal value of sensitivity to be shown directly as a measuring range.

Charge calibrators Type 541A were connected instead of transducers allowing the entire measuring chain to be calibrated with an appropriate charge signal.

Cables used in the connections were specially made for Kistler equipment. In addition to an extremely high insulation resistance, they are free from disturbing charge signals when the cables are moved around. Type 1619 cables protected by metallic tubing were used.

The outputs of the charge amplifiers were connected to the FFT analyzer (B&K, Mod. 2032). The dual channel signal analyzer (Type 2032) is flexible, easy-to-use, and is a fully self-contained two-channel FFT analysis system with 801 lines of resolution. The analyzer has a real-time speed of >5 kHz (>10 kHz in single channel). This type of FFT analyzer was selected since it is flexible, i.e. calibration, display scales, post-processing, etc. are user-definable, and functions such as signal-to-noise ratio, cross-spectra, auto-spectras, etc. are computed directly without the need for intermediate processing. It is also easy to use because the operation has all relevant control settings clearly shown on the display screen, and because complete measurement and display setups can be stored for later recall and use. The analyzer is self-contained because it has a fully instrumented front-end, built-in digital zoom, a built-in zooming signal generator and IEC/IEEE interface. Its 801-line resolution is of special importance since more modes of vibration can be identified and characterized in a signal analysis than with a conventional 250- or 400-line analyzer.

The setup was calibrated statically and dynamically. In addition, the validity of dynamic measurements was examined.

3.2.1. Static calibration

The objective of static calibration was to establish a relation between the measured value of the dynamometer and the actual value of the forces to be measured. In spite of

the fact that the piezoelectric transducers are generally used to sense dynamic quantities, the static calibration is possible because of the high insulation resistance of the load washer and because of the high input impedance provided by the charge amplifier. Thus, for any value of the load less than the maximum, in both the tangential and radial directions, the time duration of the signal is sufficiently large to permit a reading on a digital voltmeter. Static calibration of the dynamometer was carried out by applying various loads of known magnitudes measuring the output of the dynamometer, and establishing a graphical relation between the measured quantities and the applied forces. In the calibration of the dynamometer, the known loads were applied using a vertical hydraulic loading machine. To minimize the error introduced in static calibration, the charge amplifiers were set to ''long'' mode so that the time constant of the system becomes large and the rate of charge decay during calibration was reduced. The load was provided by a loading machine and was incrementally increased to a value of 10 kN. At each step, a reading was recorded. Similar readings were recorded during the unloading cycle. The latter was performed to estimate the hysteresis of the system. It was observed that the difference in the readings obtained during loading and unloading were sufficiently small to neglect this hysteresis. A typical calibration chart is shown in Fig. 3.

3.2.2. Dynamic calibration

Dynamic calibration of the dynamometer–workpiece–machine tool system has been carried out to determine the frequency band, over which the dynamometer can be used for reliable measurements. In other words, the system's resonant frequencies were determined and compared with those of the response of the cutting process.

A hammer B&K 8203 with a built-in cell has been used to supply an impulse excitation to the dynamometer–workpiece–machine tool system, while the FFT analyzer has been used for analyzing the output signals from the hammer and

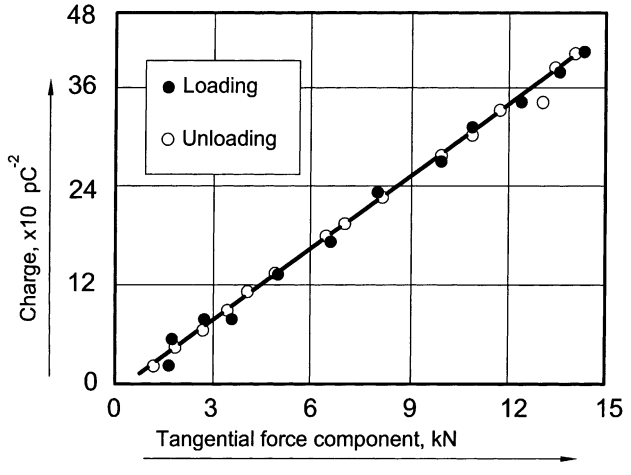

Fig. 3. Typical calibration chart (channel of the tangential force component, static calibration).

the dynamometer. First, an autospectrum of the input channel was acquired to verify that the hammer is capable of providing sufficient input energy over the frequency range of interest. Because the response is a transient function, the autospectrum was scaled to show the energy spectral density of the signal. The results clearly show that when equipped with a metal tip, the hammer provided uniform input over a broad frequency range from 0 Hz to 6 kHz (Fig. 4). A drop of less than 20 dB was tolerated following the common recommendation for resonance measurements [27]. Secondly, the frequency response function (FRF), $H_1(f)$ of the machine dynamometer–workpiece system was measured and the frequency band in which the FRF remains constant was determined. This frequency band defines the frequencies of the resultant force system, which can be measured without the introduction of any signal distortion due to the system non-linearity. Fig. 5a shows that the FRF (direct correlation) is very close to unity in the frequency range 0–1100 Hz, and Fig. 5b shows that the FRF (cross-correlation) has a constant value of 0.02 over the same range. The validity of the measurements was verified using the coherence function $\gamma^2(f)$ for the measured spectrums.

3.2.3. Spectral lines

The analyzer can capture time records consisting of 128, 256, 512, 1024 or 2048 samples. When the time records are Fourier transformed, the resultant complex spectra may have 64, 128, 256, 512 and 1024 independent lines each. However, due to employing of antialiasing filters, only 51, 100, 201, 401 or 801 lines will have the correct amplitude. It is desirable to have as many samples in a time record as possible in order to achieve better frequency resolution. Therefore, a spectrum consisting of 801 spectral lines has been selected to obtain the best frequency resolution.

3.2.4. Sampling frequency

The FFT analyzer cannot execute the Fourier transformation continuously in the course of measurements. Its internal dedicated processor must look at a time block of data to perform these calculations because it performs integrations numerically. This is the purpose of the sampling zone in the FFT analyzer. The sampling zone holds the amplified and the filtered signal in short-term memory, while voltage readings are taken. Using information stored in this memory, the processor converts the time waveform into a table of numbers. When complete, a time block of waveform data resides in the computer memory as a table of numbers that contains both amplitude and phase information. In such a format, these data are suitable for a numerical procedure. The typical spectrum analyzer takes about 50,000 readings per second on the input waveform to overcome the problem of being tracking high-frequency signals. According to the Nyquist criterion, an analyzer that has a frequency range 0–20,000 Hz must measure the voltage of the input signal faster than twice this frequency (or 40,000 Hz) to be able to see changes at 20,000 Hz. In the experiments, the sampling

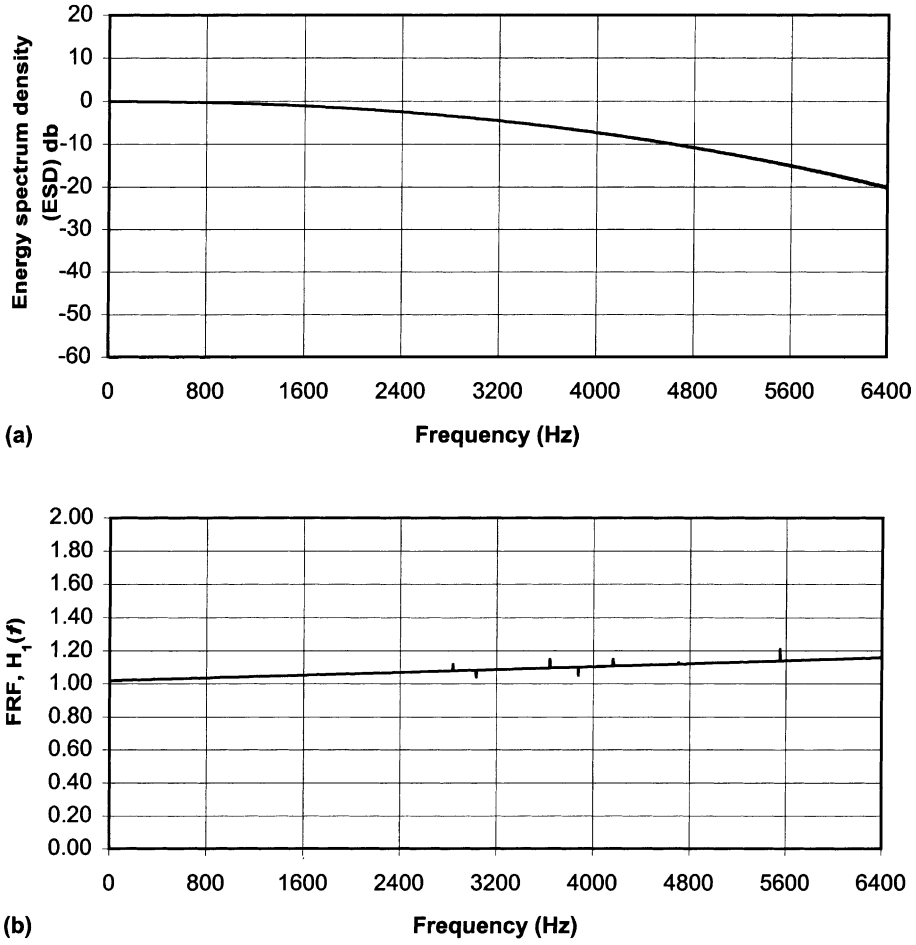

Fig. 4. Calibration of the hammer for the FRF measurements: (a) hammer response; (b) FRF values.

frequency was set to 1600 Hz to see the change in at 800 Hz that was the range of interest.

3.2.5. Averaging mode

There are three modes of averaging which can be selected to obtain suitable autospectras: (a) exponential; (b) linear; (c) peak averaging. Each mode has its application depending on the type of the signals. Exponential averaging places more emphasis on the latest spectrum. Linear averaging places equal emphasis on all of the averaged spectra. The peak averaging records the largest amplitude of each spectral line. The exponential averaging has been selected for continuous monitoring of signals, which may have relatively slow variations.

3.2.6. Averaging number

This is a number, ranging from 1 to 32,767 which determines the number of spectra that contributes to the average. The selection of this number depends on: (a) the desired accuracy; the rule of thumb here is as follows: the greater the accuracy, the higher will be the required averaging number, (b) the signal/noise ratio in the measurements and (c) the type of signal being analyzed.

For stationary signals, only a few averages are needed to obtain a good estimate. However, average of 15 has been used in the measurements to increase measuring accuracy and minimize the presence of noise in the signal. This averaging number results in an error of less than 0.5 dB and the process does not take too long [20].

3.2.7. Anti-aliasing in the signal record

Aliasing is a mirror of the high-frequency signals that appear in the lower frequency range where the high-frequency signals can form false peaks in the frequency domain. This is a consequence of the digitizing process. Aliasing frequencies appear as vertical lines in the frequency domain. They are 'ghost' images of high-frequency data. In this study, aliasing has been eliminated using two traditional methods. First, the input data were measured at the frequency that are more than twice higher than the highest frequency of interest. Secondly, used in conjunction with the first method, built-in low pass filters having cut-off frequency at about 80% of the Nyquist frequency were deployed, and the results with and without filters were compared. Typically for 2048 points, 801 frequency lines were displayed.

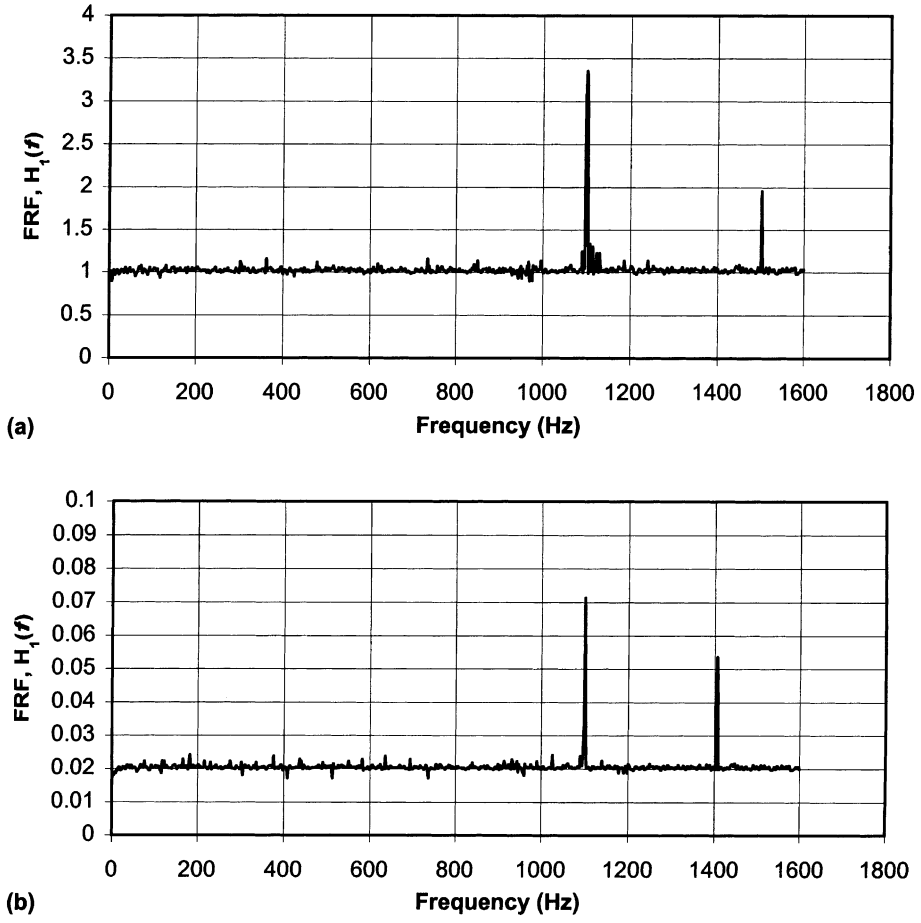

Fig. 5. FRF when the input excitation was along the direction of the power component of the cutting force: (a) direct correlation; (b) cross-correlation.

3.2.8. Windowing the data

Windowing the data is one of the most important parameters. In the FFT analyzer, the digital sampling takes place during discrete blocks of time. Performing a numerical analyses, the FFT analyzer assumes that the signal which exists in that block of time also exists before and after the current sampling time. As mentioned, processing by time blocks allows real-time data acquisition. Therefore, it is not possible for the analyzer to wait for an extended time period to verify if the signal is periodic. The Fourier transformation, however, should make an assumption of periodicity to start the acquisition process. In doing so, it can produce a leakage error if the actual signal does not match at the beginning and end of the current time block. This leakage is undesirable since it may hide low amplitude signals causing distortions in the resultant spectrum. To avoid significant leakage, the input data is weighted with a mathematical function that favors the data in the center of the time block and reduces the data at both ends to zero. There are many useful window functions which can be used such as rectangular, Hanning, hamming, Kaiser–Bessel and flat top. Because the cutting force signal is proven to be wear stationary [20], the Hanning window was selected because it meets these requirements [27].

3.3. Cutting force–cutting speed relationships

In the first series of experiments, the mean values of the power component of the cutting force P_z (for simplicity hereafter will be referred to as the cutting force) have been measured at different cutting speeds V and depth of cut t under a constant feed $s = 0.12\,\text{mm/rev}$. The results are shown in Table 1.

Following the traditional way suggested in earlier studies [2,4,5,20], the cutting force–cutting speed relationships were expressed by the simple power curve relation

$$P_z = CV^x \tag{1}$$

where C and x are constants.

Using the obtained experimental results (Table 1), the following relationships can be written

$$P_z = 53.94V^{-0.1} \quad \text{when } t = t_1 \tag{2}$$

$$P_z = 193.13V^{-0.1} \quad \text{when } t = t_2 \tag{3}$$

$$P_z = 427.79V^{-0.1} \quad \text{when } t = t_3 \tag{4}$$

This study, however, suggests another type of representation of the experimental results. The experimental points from Table 1 were placed in the orthogonal coordinate system

Table 1
Experimental results (series No. 1 of experiments)

Cutting speed V (m/s)	Cutting force, P_z (N)		
	$t_1 = 0.1$ mm	$t_2 = 0.5$ mm	$t_3 = 1.0$ mm
0.07	84	328	506
0.11	75	244	469
0.23	47	206	469
0.29	38	206	375
0.46	38	169	375
0.58	56	169	394
0.72	47	178	469
0.92	41	178	450
1.15	47	169	469
1.82	56	187	431
2.30	56	187	469
2.63	60	178	431
4.60	38	169	375
5.76	53	187	366

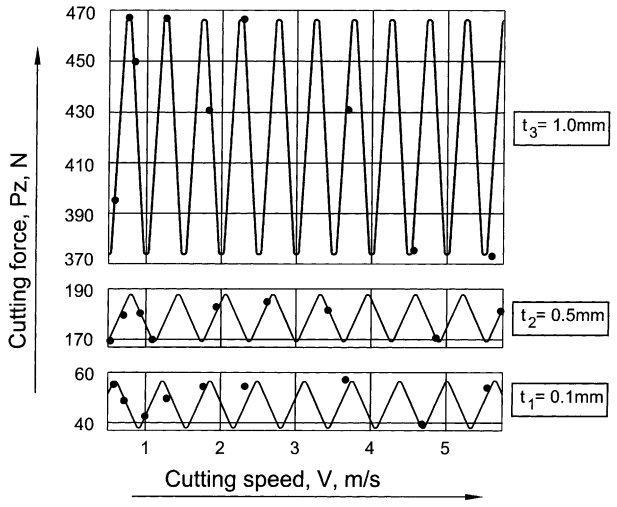

Fig. 6. Experimental results represented as sinusoidal periodic data in the coordinate system "V–P_z": (a) $t_1 = 0.1$ mm; (b) $t_2 = 0.5$ mm; (c) $t_3 = 1.0$ mm.

"V–P_z". With regards to the aforementioned wave nature of deformation, these points were considered as sinusoidal periodic data (Fig. 6) that can be represented mathematically as

$$P_z = P_{z0} + P_{za} \sin\left[\frac{2\pi}{l_V}(V + F_V)\right] \quad (5)$$

where P_{z0} is the mean of the sine wave, P_{za}, l_V and F_V are its amplitude, wavelength and initial phase, respectively.

The proposed representation of the data of Table 1 results in the following models

$$P_z = 47 + 10 \sin\left[\frac{2\pi}{0.56}(0.056 + V)\right] \quad \text{when } t = t_1 \quad (6)$$

$$P_z = 422 + 50 \sin\left[\frac{2\pi}{0.40}(0.095 + V)\right] \quad \text{when } t = t_2 \quad (7)$$

$$P_z = 178 + 11 \sin\left[\frac{2\pi}{0.50}(0.049 + V)\right] \quad \text{when } t = t_3 \quad (8)$$

The results of experiments have also shown that the wavelength of the sine wave l_V depends entirely on the properties of the work material under a given cutting regime and tool geometry. The sinusoidal character of the experimental results is explained in the next section.

3.4. Coherent energy waves

In the cutting process, a significant part of the input energy converts into heat, which is then transferred to the chip, the workpiece and the cutting tool. The part of the heat transferred into the workpiece is of prime concern here because it directly affects the cutting force [4,5,20].

Consider the turning of a bar and the corresponding cutting tool trajectory as shown in Fig. 7a and b, respectively. Further consider a microvolume of the work material located at point 2 on the tool trajectory (Fig. 7b) at the instant when the tool passes this point. The change in the internal energy of the microvolume (dU) may be thought of as the sum of the mechanical work done by the external forces (dA) applied by the tool and the residual heat from the identical volume located on the neighboring trajectory of the cutter (dQ) (from point 1, Fig. 7b), thus

$$\mathrm{d}U = \mathrm{d}Q + \mathrm{d}A \quad (9)$$

As seen, the residual heat dQ in Eq. (9) is considered a positive term because this heat is transferred into the microvolume at point 2 (when the cutting tool is there) from the decaying heat source of point 1 (the preceding position of the cutting tool) if and only if the velocity of heat conduction in the workpiece is equal to and greater than the translation speed of the cutting system along the feed direction (the x-direction in Fig. 7). This velocity is known as the feed rate

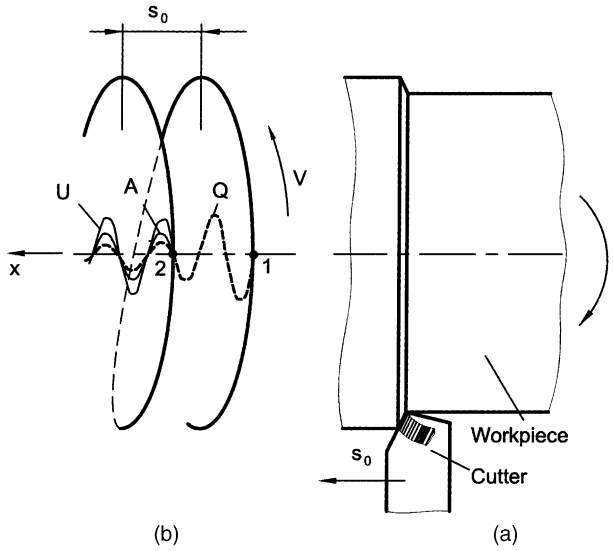

Fig. 7. External bar turning (a) and the trajectory of the cutting tool (b).

and can be calculated knowing the rotational speed of the workpiece n (in rev/minute) and the feed per revolution s_0, as $V_s = ns_0$. When a moving heat source is considered the velocity of heat transfer by conduction is completely characterized by the Peclet number [20]

$$Pe = \frac{va}{w} \tag{10}$$

Here v is the velocity of a heat source (m/s). For the considered case, the velocity of a heat source is equal to the feed velocity V_s, a is the uncut chip thickness (m), w the thermal diffusivity of the work material (m^2/s). If $Pe > 10$, then a source moves faster than heat that can be transferred and if $Pe \leq 10$ the source moves slower thus the residual heat affects the work material ahead of the tool. In metal cutting, the translation speed V_s is relatively low and falls in a range from 0.01 to 1 mm/s so that $Pe \ll 10$. In the current case, for example, the parameters are as follows: $s = 0.12$ mm/rev, $V_s = 0.74$ mm/s, $t = 0.5 \times 10^{-3}$ m, $w = 6.75 \times 10^{-6}$ m^2/s. As such, $Pe = 0.055$. Therefore, there is no contradiction with the laws of thermodynamics in Eq. (9) — first heat enters to the less heated zone (point 2, Fig. 7b) and then the cutting tool (as a heat source) moves there, thus the residual heat in Eq. (9) is positive.

Because the residual heat dQ in Eq. (9) is a part of the mechanical energy converted into heat at point 1 of the tool trajectory (Fig. 7b), the frequencies of the heat and the deformation longitudinal waves should be identical because they are generated by the same source, namely the cutting tool. As indicated in [24], the interaction of such longitudinal waves results in the reinforcement of energy flux U when these waves in-phase, i.e. when the path difference represented in the considered case by the feed s, is

$$s = \tfrac{1}{2}2kl, \quad k = 0, 1, 2 \ldots \tag{11}$$

where l is the wavelength.

In contrast, when the path deference is

$$s = \tfrac{1}{2}(2k+1)l, \quad k = 0, 1, 2 \ldots \tag{12}$$

then these waves have opposite phase which results in their interference.

It follows from Eqs. (11) and (12) that if the feed is kept invariable, the reinforcement and interference of the total energy flux are possible only when the wavelength is a function of the cutting speed, i.e. when $l = f(V)$ is the case. In order to prove this, consider the extremes of the sinusoidal function defined by Eq. (5). If certain ith crest of this function takes place when $s = kl_i$, then the next crest appears when the number of the waves increases by 1, i.e. when $s = (k+1)l_{i+1}$. Consequently,

$$l_{i+1} = \frac{l_i}{1 + l_i/s} \tag{13}$$

Eq. (13) enables one to obtain the expression for the wavelength of an energy wave occurring at other cutting speed V_2 that differs from the original speed V_1 on an even number of wavelengths in Eq. (5) as

$$l_q = \frac{sl_1}{s + ql_1} \tag{14}$$

where q is the number of wavelengths by which speed V_2 exceeds speed V_1 ($V_2 = qV_1$), l_1 the wavelength corresponding to the cutting speed V_1.

Since q for any speed V can be calculated as

$$q = \frac{V - V_1}{l_V} \tag{15}$$

the wavelength l corresponding to this speed is

$$l = \frac{1}{1/l_1 + (V - V_1)/(l_V s)} \tag{16}$$

In [20], metal cutting is defined as purposeful failure or fracture of the workpiece material, and thus the energy necessary for such failure should be supplied to the machining zone through the cutter. According to the Von Mises criterion of failure with the physical meaning given by Hencky, the failure occurs when the distortion energy (the total strain energy per unit volume) reaches a critical value [25]. It is important to note here that the criterion does not specify a particular kind of energy. Because this critical value depends only on the properties of workpiece material, i.e. a constant for a given workpiece material, the interaction of the above considered longitudinal waves should affect the amount of the external mechanical energy A consumed by the cutting system. This is proven by the apparent variation of the cutting force P_z since

$$A = P_z V \tau \tag{17}$$

where τ is the time of consideration.

The phenomenon of the interaction of the deformation and heat longitudinal waves was additionally examined as follows. The interaction of the waves takes place due to the fact that these waves are coherent. Therefore, if the coherence of the waves is disturbed, the interaction should not be observed.

The second series of experiments was carried out using face cutting (Fig. 8a). Table 2 lists ranges of the cutting parameters used in the test. Other parameters of the cutting system and the measuring rig were kept the same.

The experimental results obtained in this test show that no force variation has been observed through a considerably wide range of cutting conditions. This result is explained as follows.

Table 2
Ranges of values of cutting parameters for the end turning tests

Parameter	Low value	High value
Workpiece diameter (mm)	60	120
Cutting speed (m/s)	0.15	4.00
Feed (mm/rev)	0.07	0.25
Depth of cut (mm)	0.10	3.00

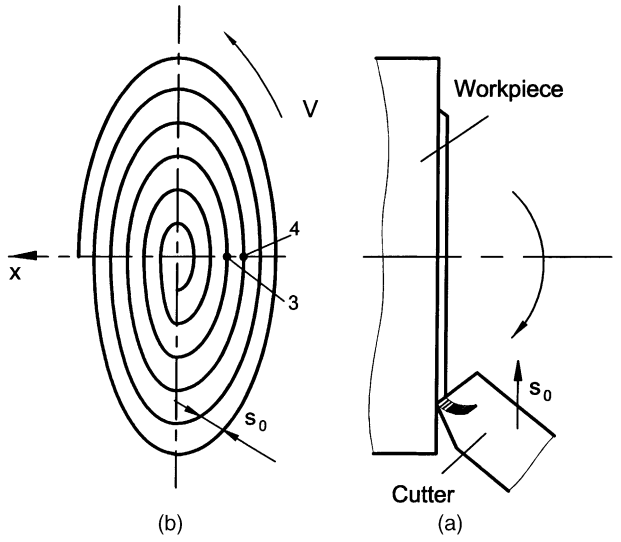

Fig. 8. Face cutting (a) and trajectory of the cutting tool (b).

In face cutting, the cutting speed is not constant, but differs for each successive point of the tool trajectory (Fig. 8b). Therefore, the heat wave generated on the neighboring trajectory of the cutting tool (point 3) does not affect the cutting force (energy consumption) on the current trajectory (point 4) because this heat wave has been formed at different cutting speed and, therefore, the deformation and the heat waves are not coherent. Therefore, the results of the experiment prove that, on one hand, the cutting speed affects the wavelength and, on the other hand, the interaction of the waves is a real phenomenon of the cutting process.

3.5. Influence of the feed

Changing the feed can vary the wave path. However, the cutting force P_z is affected not only by the wave-interaction force component $P_s(s)$, but also by the force component which depends on the uncut chip thickness $P_0(s)$. Mathematically, it can be represented as

$$P_z = P_0(s) + P_s(s) = P_0(s) + P_a \sin\left[\frac{2\pi}{l_s}(s + F_s)\right] \qquad (18)$$

The third series of experiments was carried out to determine the components of Eq. (18). The test conditions and the measuring setup were identical to those used before. Longitudinal turning was conducted on bars of 60 mm diameter. The depth of cut of 0.1 mm was kept constant in the experiments. The feed varied in the range 0.070–0.130 mm/rev for each of the six cutting speeds ($V = 2.9$, 2.3, 1.8, 1.4, 1.2 and 0.9 m/s) used in the tests.

The experimental results are shown in Fig. 3. Using these experimental results, $P_0(s)$ was determined in each experiment as the mean of the corresponding sine wave. After that, the component $P_s(s)$ was determined from Eq. (18) as

$$P_s = P_z - P_0(s) \qquad (19)$$

The functions $P_s = f(s)$, shown in Table 3, were determined using a curve fitting computer program as follows. The experimental points were mapped in the coordinate system "P_s–s_0" as shown in Fig. 9. Then, an appropriate sine wave of a general form

$$P_s(s) = P_a \sin\left[\frac{2\pi}{l_s}(s + F_s)\right] \qquad (20)$$

was selected for each set of data by the computer. In doing this, the wavelength for the cutting speeds used in the experiments was determined. Table 4 shows the comparison between the experimentally determined and the calculated wavelengths. The calculations were performed using Eq. (14) and the lowest speed $V_1 = 0.9\,\text{m/s}$ ($l_1 = 7.8\,\mu\text{m}$ and $l_V = 0.56\,\mu\text{m}$) was selected as the reference point.

The experimental results reveal two important aspects. First, the interaction between the deformation and the heat wave takes place under different feeds. Secondly, a good agreement between the experimental and the calculated results proves the basic concept.

3.6. Influence of other parameters of the machining process

A special series of experiments was carried out to prove that the characteristics of the energy waves do not correlate with the frequency of the spindle rotation, with the vibrations

Table 3
Experimental results (series No. 3 of experiments)

s (mm/rev)	$V = 2.9\,\text{m/s}$		$V = 2.3\,\text{m/s}$		$V = 1.8\,\text{m/s}$		$V = 1.4\,\text{m/s}$		$V = 1.2\,\text{m/s}$		$V = 0.9\,\text{m/s}$	
	P_z (N)	P_s (N)	P_z (N)	P_z (N)	P_z (N)	P_s (N)	P_z (N)	P_s (N)	P_z (N)	P_s (N)	P_z (N)	P_s (N)
0.070	75	−2.84	56.2	−3.05	56.2	−0.01	0.070	−2.81	54.4	2.11	56.2	3.98
0.074	84	3.91	60.0	−2.06	60.0	1.67	0.074	4.29	58.1	3.40	56.2	1.54
0.084	81	−4.70	71.2	2.29	65.6	2.11	0.084	2.37	61.9	1.05	52.5	−8.32
0.097	94	1.00	76.9	−1.06	71.2	1.00	0.097	−1.25	71.2	2.48	76.9	8.11
0.110	103	2.68	84.4	−2.53	75.0	−1.98	0.110	2.63	75.0	−1.74	80.6	3.92
0.120	103	−2.94	93.7	−0.05	84.4	2.21	0.120	−3.04	78.7	−4.07	88.1	5.30
0.130	112	0.40	103.1	2.42	90.0	2.26	0.130	4.41	93.7	4.82	96.6	6.69
	$P_0 = 38.5 + 562s$		$P_0 = 11 + 690s$		$P_0 = 20 + 518s$		$P_0 = 10 + 567s$		$P_0 = 9.5 + 611s$		$P_0 = 9.5 + 611s$	

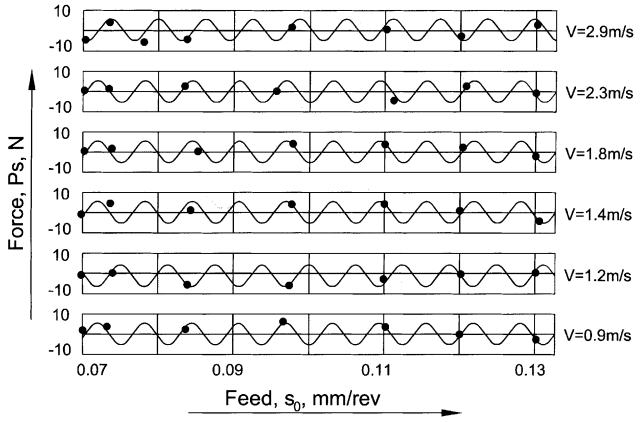

Fig. 9. Sine wave approximations of the experimental data in the coordinate system "P_s–s_0".

generated by the drive unit and other rotating and moving machine's components. Owing to the fact that such correlation may dramatically affect the results, two independent sets of experiments were carried out.

Table 4
Comparison between the experimentally determined and the calculated wavelengths

Cutting speed (m/s)	Wavelength (μm)	
	Experiment	Calculation
0.9	7.8	7.800
1.2	7.6	7.780
1.4	7.1	7.348
1.8	7.0	7.033
2.3	6.5	6.723
2.9	6.3	6.336

The first set of experiments included the comparison of the frequencies from the autospectras obtained at the corresponding speeds with that obtained experimentally for the energy waves (Table 4, Fig. 10). The comparison reveals that no correlation exists.

The second set included the cutting force determination at the cutting speeds used in earlier experiments under different combinations of the spindle rpm and the workpiece diameter

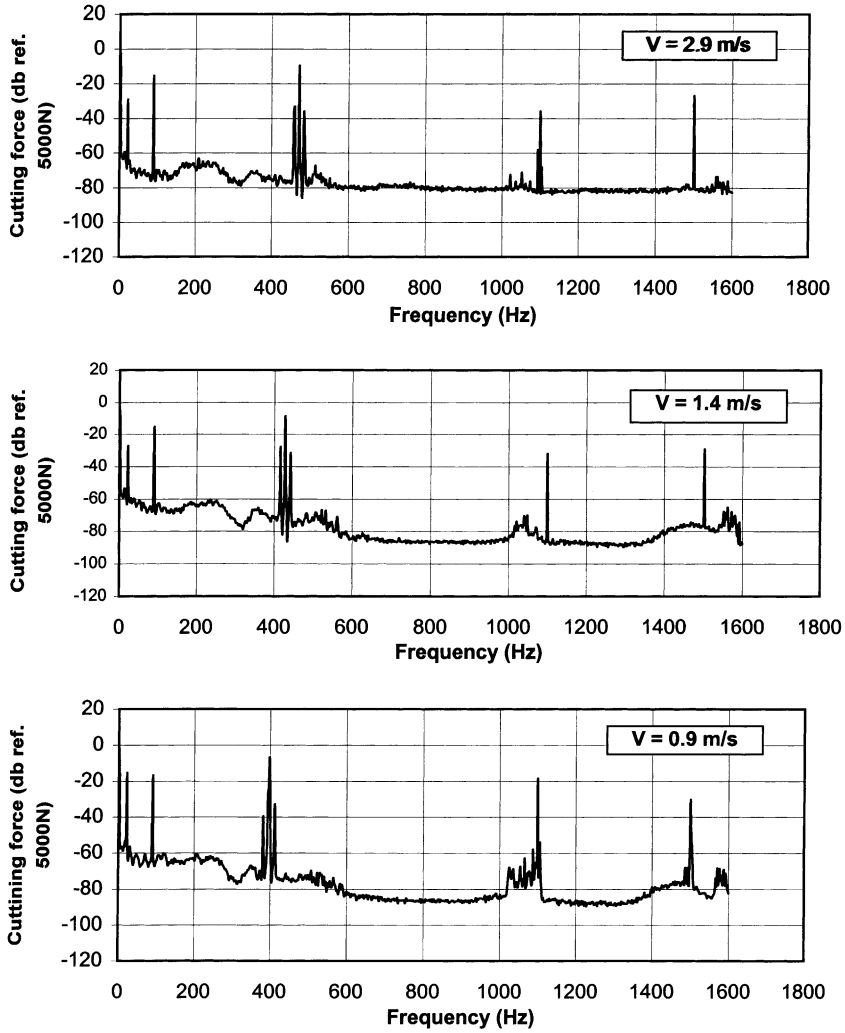

Fig. 10. Autospectras for the cutting force for different cutting speeds. Workpiece material — AISI 4140.

(Fig. 10). It is understood that different structural frequencies have been involved. However, no correlation was observed.

4. Results and discussion

High-energy rate cutting results in the generation of the deformation and heat waves. Since these waves are generated by the same source, namely by the deforming tool, they are coherent thus their interaction takes place in the process. This interaction affects the required amount of external energy since, according to the Von Mises criterion of failure with physical meaning given by Hencky, the critical value of the distortion energy (the total strain energy per unit volume) is constant for a given workpiece material. The existence of the discussed interaction offers a novel approach to the selecting of the optimal process regime for high-energy rate deforming processes, in general, and for cutting, in particular. This regime should be selected so that the interaction of energy waves results of their reinforcement at the point of cutting (deforming) that significantly reduces the energy needed to accomplish the process. At higher strain rates and cutting speeds, the benefits of the proposed approach are significant.

Another important aspect is that the results of the present study clearly demonstrates that the interpretation of the experimental results in metal cutting should not be accomplished without accountings for wave effects. Averaging of the cutting force signal, use low cut-off frequency strain gages as the force transducers in experimental studies (for example, [28]) leads to ignoring the essence of high-energy deforming processes. Moreover, it should not be forgotten that metal cutting results in purposeful fracture of the layer to be removed [20]. Since chip formation process is cyclical [20,22], fracture occurs in each cycle so that the workpiece is subjected to the application of a series of successive high strain rate microimpulses. Therefore, the known results of the mechanical testing of materials at high strain rates where a single shock load is applied may not be fully applicable in metal-cutting studies.

The experiments reveal that:

- When the process regime and the tool configuration are kept constant, the wavelength of the deformation wave depends mainly on the properties of the workpiece material.
- Interaction between the deformation and the heat waves takes place when the process speed and feed are varied.
- Characteristics of the deformation wave do not correlate with the vibration characteristics of the experimental setup.

The study offers a simple experimental method to determine the parameters of the deformation wave. The results may be used for the selection of the process regime corresponding to the minimum energy consumption.

References

[1] G. Dieter, Mechanical Metallurgy, 3rd Edition, McGraw-Hill, New York, 1986.
[2] P.L.B. Oxley, Mechanics of Machining: An Analytical Approach to Assessing Machinability, Wiley, New York, 1989.
[3] M.E. Merchant, Mechanics of the metal cutting process, J. Appl. Phys. 16 (1945) 267–275.
[4] M.C. Shaw, Metal Cutting Principles, Clarendon Press, Oxford, 1984.
[5] N.N. Zorev, Metal Cutting Mechanics, Pergamon Press, Oxford, 1966.
[6] F. Lira, E.G. Thomsen, Metal cutting as a property test, ASME J. Eng. Ind. 89 (1967) 498–503.
[7] V.P. Astakhov, A treatise on material characterization in the metal cutting process. Part 1: a novel approach and experimental verification, J. Mater. Process. Technol. 96 (1999) 22–33.
[8] E. Usui, Progress of predictive theories in metal cutting, JSME Int. J. III 31 (2) (1988) 363–369.
[9] S. Kobayashi, E.G. Thomsen, Metal-cutting analysis. I: re-evaluation and new method of presentation of theories, ASME J. Eng. Ind. 90 (1962) 63–70.
[10] J.H.L. Thé, R.F. Scrutton, The stress-state in the shear zone during steady state machining, ASME J. Eng. Ind. 101 (1979) 211–216.
[11] B. Zhang, A. Bagchi, Finite element simulation of chip formation and comparison with machining experiment, ASME J. Eng. Ind. 116 (1994) 289–297.
[12] D. Kececioglu, Shear-zone size, compressive stress, and shear strain in metal-cutting and their effects on mean shear-flow stress, ASME J. Eng. Ind. 81 (1960) 79–86.
[13] K. Ocusima, K. Hitomi, An analysis of the mechanism of orthogonal cutting and its application to discontinuous chip formation, ASME J. Eng. Ind. 82 (1961) 545–556.
[14] R. Stevenson, D.A. Stephenson, The mechanical behavior of zinc during machining, ASME J. Eng. Mater. Technol. 117 (1995) 173–178.
[15] R.I. King (Ed.), Handbook of High-speed Machining Technology, Chapman & Hall, New York, 1985.
[16] C. Spaans, A treatise of the streamlines and the stress, strain, and strain rate distributions, and on stability in the primary shear zone in metal cutting, ASME J. Eng. Ind. 94 (1972) 690–696.
[17] B.E. Klamensky, S. Kim, On the plane stress to plane strain transition across the shear zone in metal cutting, ASME J. Eng. Ind. 110 (1988) 322–325.
[18] A.J. Shih, Finite element simulation of orthogonal metal cutting, ASME J. Eng. Ind. 117 (1995) 84–92.
[19] X. Song, Strain-hardening and thermal-softening effects on shear angle prediction: new model development and validation, ASME J. Eng. Ind. 117 (1995) 28–32.
[20] V.P. Astakhov, Metal Cutting Mechanics, CRC Press, Boca Raton, FL, 1998.
[21] A.G. Atkins, Y.W. Mai, Elastic and Plastic Fracture: Metals, Polymers, Ceramics, Composites, Biological Materials, Ellis Horwood, Chichester, UK, 1985.
[22] V.P. Astakhov, S.V. Shvets, A system concept in metal cutting, J. Mater. Process. Technol. 79 (1–3) (1998) 189–199.
[23] C. Truesdell, W. Noll, The Non-linear Field Theories of Mechanics, Handbuch der Physik, Vol. III, No. 3, Springer, Berlin, 1965.
[24] J. Engelbrecht, Nonlinear Wave Processes of Deformation in Solids, Pitman, London, 1983.
[25] W. Johnson, P.B. Mellon, Engineering Plasticity, Ellis Horwood, Chichester, UK, 1983.
[26] J. Buchar, Z. Bilek, F. Dusek, Mechanical Behavior of Metals at Extremely High Strain Rates, Trans Tech Publications, Switzerland, 1986.
[27] R.B. Randall, Frequency Analysis, Larsen, Glostrup, Denmark, 1987.
[28] G. Sutter, A. Molinari, L. Faure, D. Dudzinski, An experimental study of high speed orthogonal cutting, ASME J. Manuf. Sci. Eng. 120 (1998) 169–172.